Mon. Not. R. Astron. Soc. **304,** 35–46 (1999)

Extended gas in Seyfert galaxies: near-infrared observations of NGC 2110 and Circinus

Thaisa Storchi-Bergmann,[1⋆] Cláudia Winge,[1,2⋆] Martin J. Ward[3⋆] and Andrew S. Wilson[4,2⋆]

[1]*Instituto de Física, UFRGS, Campus do Vale, CP 15051, P. Alegre, RS, Brazil*
[2]*Space Telescope Science Institute, 3700 San Martin Drive, Baltimore, MD 21218, USA*
[3]*Department of Physics and Astronomy, University of Leicester, University Road, Leicester LE1 7RH*
[4]*Astronomy Department, University of Maryland, College Park, MD 20742, USA*

Accepted 1998 November 5. Received 1998 November 3; in original form 1998 July 8

ABSTRACT

We present results of near-IR long-slit spectroscopy in the *J* and *K* bands of the Seyfert 2 galaxies NGC 2110 and Circinus. Our goal is to investigate the gaseous distribution, excitation, reddening and kinematics, looking for signatures of the molecular torus hypothesized in unified models to both obscure and collimate the nuclear radiation. The two galaxies show extended emission in the IR emission lines [Fe II]λ1.257 μm, Pa β and $H_2 v = 1–0$ S(1), both along the major axis of the galaxy disc and perpendicular to it. In NGC 2110, the emission-line ratio [Fe II]/Pa β increases towards the nucleus, where its value is ≈7. Further, the nuclear [Fe II] and Pa β lines are broader (FWHM $\simeq$ 500 km s^{-1}) than the H_2 line (FWHM $\leq$ 300 km s^{-1}). Both these results suggest that shocks, driven by the radio jet, are an important source of excitation of [Fe II], while the H_2 excitation is dominated by X-rays from the nucleus. Br γ is only observed at the nucleus, where H_2/Br $\gamma \approx 3$. In the case of Circinus, both [Fe II]/Pa β and H_2/Br γ decrease from ≈ 2 at 4 arcsec from the nucleus to nuclear values of ≈ 0.6 and ≈ 1, respectively, suggesting that the starburst dominates the nuclear excitation, while the active galactic nucleus (AGN) dominates the excitation further out ($r \geq 2$ arcsec). For both galaxies, the gaseous kinematics are consistent with circular rotation in the plane of the disc. Our rotation curves suggest that the nucleus (identified with the peak of the IR continuum) is displaced from the kinematic centre of the galaxies. This effect has been observed previously in NGC 2110 based on the kinematics of optical emission lines, but the displacement is smaller in the infrared, suggesting the effect is related to obscuration. The continuum $J - K$ colours indicate a red stellar population in NGC 2110 and a reddened young stellar population in Circinus, outside the nucleus. Right at the nucleus of both galaxies, the colours are redder, apparently a result of hot dust emission, perhaps from the inner edge of a circumnuclear torus. In NGC 2110, the signature of the hot dust emission is particularly clear in the *K* band, being seen as an additional component superimposed on the continuum observed in the *J* band.

Key words: galaxies: active – galaxies: individual: NGC 2110 – galaxies: individual: Circinus – galaxies: ISM – galaxies: seyfert – infrared: galaxies.

1 INTRODUCTION

The nuclear regions of Seyfert 2 galaxies are dusty environments, as revealed by red nuclear colours in optical imaging and large Balmer emission-line ratios in spectroscopic studies (e.g. Ward et al. 1987; Storchi-Bergmann, Wilson & Baldwin 1992; Mulchaey et al. 1994, Storchi-Bergmann, Kinney & Challis 1995; Simpson et al. 1996b; Cid-Fernandes, Storchi-Bergmann & Schmitt 1998). Although such reddening may be caused by large-scale dust in the central regions of the host galaxies, dust on smaller scales is believed to be concentrated in an optically thick molecular torus with dimensions of tens of pc and surrounding the nuclear engine (e.g. Antonucci & Miller 1985; Antonucci 1993). This torus both obscures the nucleus from direct view and collimates the ionizing radiation, giving origin to the 'ionization cones' observed in Seyfert 2 galaxies (e.g. Mulchaey, Wilson & Tsvetanov 1996). Evidence for reradiation

⋆Visiting Astronomer at the Cerro Tololo Interamerican Observatory, operated by the Association of Universities for Research in Astronomy, Inc. under contract with the National Science Foundation.

from hot dust emitting in the near-IR has been found, among others, by McAlary & Rieke (1988), Sanders et al. (1989) and Alonso-Herrero, Ward & Kotilainen (1996).

In order to penetrate the dust layers in Seyfert 2 galaxies, it is necessary to observe in the infrared region of the spectrum. At $\lambda \approx 2\mu$m, $A_K \approx A_V/10$, so near-IR observations can reach deeper into the nuclear region than optical observations. In addition, if there is warm molecular hydrogen near the nucleus, emission from the vibrational–rotational transitions of molecular hydrogen [such as H_2 $v = 1$–0 S(1) at rest wavelength 2.122 μm] should be strong. If an H_2-emitting disc-like structure could be detected elongated perpendicular to the ionization cone or radio axis, this would provide very strong support for the unified model. Narrow-band imaging studies by Blietz et al. (1994) have indeed shown that in NGC 1068 the H_2 line emission is spatially extended almost perpendicular to the cone. Similar results have been found for NGC 4945 (Moorwood et al. 1996).

With these issues in mind, we have obtained long-slit spectra in the *J* and *K* bands of a number of Seyferts with anisotropic high-excitation optical emission, which, in the unified model, is a result of ionization and excitation by nuclear radiation collimated by the torus. We present in this work the results for NGC 2110 and Circinus, the two galaxies for which we were able to detect IR emission lines at the largest distances from the nuclei.

NGC 2110 is an early-type Seyfert 2 galaxy discovered through its X-ray emission (Bradt et al. 1978). Narrow-band images show high-excitation gas extending up to 10 arcsec from the nucleus (Wilson, Baldwin & Ulvestad 1985; Mulchaey et al. 1994), in a similar direction to a jet-like radio source at position angle (PA) 10° (Ulvestad & Wilson 1983). Wilson et al. (1985) and Wilson, Baldwin & Ulvestad (1985), using optical long-slit spectroscopy, have found extended ionized gas in normal rotation about the photometric minor axis, but with the kinematic centre displaced ≈1.7 arcsec south of the optical continuum nucleus. Adopting a distance to NGC 2110 of 31.2 Mpc (using the systemic velocity from Wilson & Baldwin 1985, for $H_0 = 75$ km s^{-1}), we obtain a scale of 151 pc arcsec^{-1}.

The Circinus galaxy is a nearby (∼ 4 Mpc) spiral (Freeman et al. 1977) with a nuclear spectrum characteristic of both starburst and Seyfert activity (Moorwood & Oliva 1988, 1990). It contains the closest known ionization cone and a circumnuclear starburst ring (Marconi et al. 1994). It is a strong H_2O megamaser emitter, and shows radio lobes approximately orthogonal to the galactic plane (Elmoutie et al. 1995). Maiolino et al. (1998) present *H* and *K* images of the inner 13arcsec × 13 arcsec, narrow-band images of the central 5 arcsec × 5 arcsecand a study of the stellar kinematics using near-IR absorption bands. Davies et al. (1998) present narrow-band images in [Fe II]λ1.64 μm and H_2 $v = 1$–0 S(1), as well as radio continuum maps at 3 and 6 cm. Our adopted distance of 4 Mpc (Freeman et al. 1977) corresponds to a scale of 19 pc arcsec^{-1}.

2 OBSERVATIONS

Long-slit spectra of NGC 2110 and Circinus in the *J* and *K* bands were obtained using the Infrared Spectrograph (IRS) on the 4-m telescope of the Cerro Tololo Interamerican Observatory on the nights of 1995 November 1 and 2 and 1996 March 2. The scale of the 256×256 InSb detector was 0.363 arcsec per pixel, and the useful slit length was 15 arcsec. Two gratings were used: one with 75 line mm^{-1}, and resolution $R \approx 700$ (∼4 pixels), hereafter the LR grating, and the other with 210 line mm^{-1}, and $R \approx 2000$, hereafter the HR grating. The corresponding velocity resolutions are ≈ 400 and 150 km s^{-1}, respectively. The slit width was either 1.1 arcsec or 1.7 arcsec, depending on the seeing.

NGC 2110 was observed along two position angles: PA = 170°, which is close to both the major axis of the inner isophotes in the narrow-band [O III] image of Mulchaey et al. (1994) and the major axis of the galaxy disc, and along the perpendicular direction, at PA = 80°. Circinus was observed along the approximate axis of the radio lobes at PA = −66°, and along the approximate galaxy major axis at PA = 24°. A log of the observations is presented in Table 1.

Wavelength calibrations in the *J* and *K* bands were obtained using an He Ar lamp and OH sky lines, respectively. The reduction was performed using IRAF through scripts kindly made available by Richard Elston (available at the CTIO ftp archive). One-dimensional spectra were extracted by binning together 2 pixels (0.73 arcsec), except for the outermost locations where 4 pixels (1.46 arcsec) were co-added to improve the signal-to-noise ratio (S/N). The atmospheric absorption features were removed using spectra of nearby stars bracketing the galaxy observations; each extracted spectrum was divided by the normalized spectrum of a star (or the average between the spectra of two stars, one observed before and the other after the galaxy). The spectra were then flux-calibrated using observations of standard stars from Elias et al. (1982).

3 RESULTS

3.1 NGC 2110

3.1.1 Emission-line profiles

Sequences of *J*- and *K*-band spectra obtained with the LR grating are presented in Figs 1 (PA = 170°) and 2 (PA = 80°). The higher dispersion spectra obtained with the HR grating are shown in Fig. 3. The strongest emission line in the *J* band is [Fe II]λ1.257 μm,

Table 1. Log of observations.

Object	Date	PA(°)	Band (μm)	Grating (line mm^{-1})	Exp. time (sec)	Slit width (arcsec)
NGC 2110	1995 November 1	170	J(1.24-1.35)	75	2400	1.1
	1995 November 2	80	K(2.07-2.24)	75	2160	1.1
	1995 November 2	170	K(2.07-2.24)	75	1800	1.1
	1996 March 2	170	J(1.26-1.30)	210	1800	1.7
Circinus	1996 March 2	24	J(1.24-1.29)	210	1800	1.7
	1996 March 2	−66	J(1.24-1.29)	210	800	1.7
	1996 March 2	−66	K(2.12-2.18)	210	800	1.7
	1996 March 2	24	K(2.12-2.18)	210	800	1.7

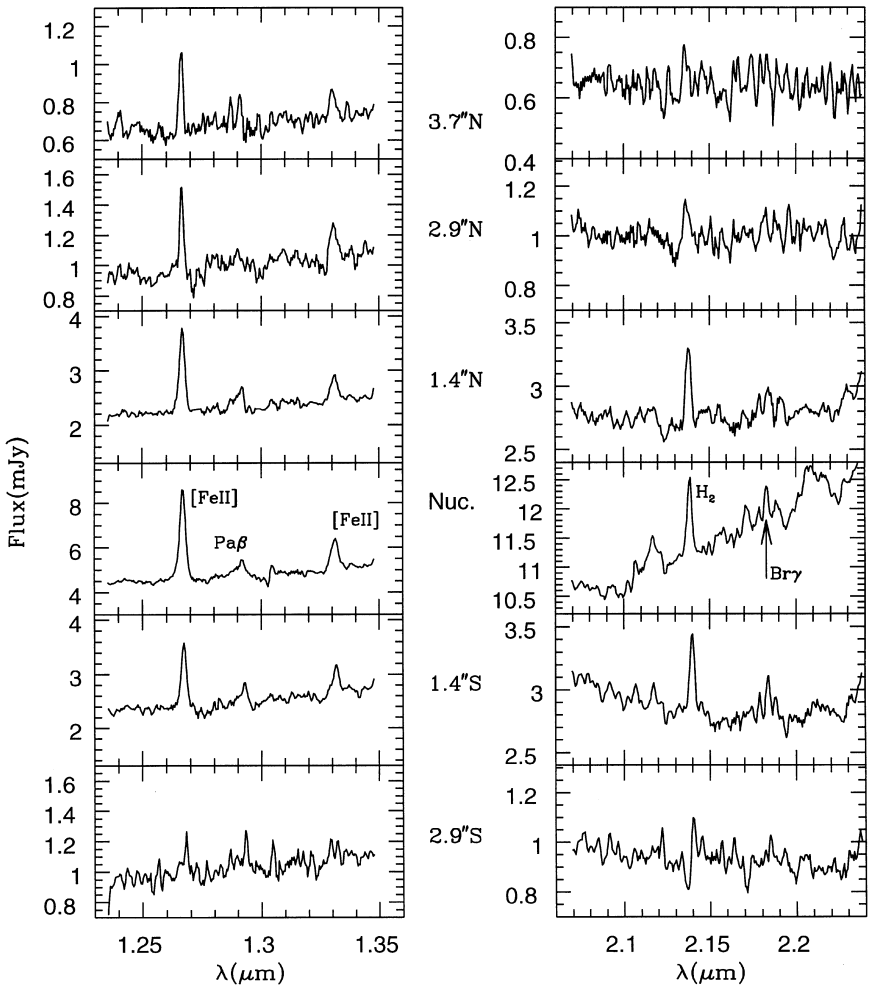

Figure 1. *J*- and *K*-band spectra of NGC 2110 at $R \approx 700$ along the radio axis at PA = 170°, after binning two pixels (0.73 arcsec) together. The distance from the nucleus is indicated.

followed by [Fe II]λ1.321 and Pa β. The profiles of [Fe II]λ 1.257 and Pa β are better defined in the higher dispersion spectrum of Fig. 3. We find that Pa β is blended with [Fe II]λ1.279 μm, which has a predicted flux of 7 per cent of that of [Fe II]λ1.257 μm. Although the profile of [Fe II]λ1.279 μm is not well defined (because of its low S/N), its full width at half maximum (FWHM) is similar to that of [Fe II]λ1.257 μm, and the observed wavelength and flux agree with the expected values.

[Fe II]λ1.257-μm emission is observed up to ≈5 arcsec to the north and ≈3 arcsec to the south, being stronger to the north, where both the radio (Ulvestad & Wilson 1983) and optical high-excitation line ([O III]) emission are stronger (Wilson et al. 1985; Mulchaey et al. 1994).

In the *K* band, H_2 $v = 1$–0 S(1) is clearly detected to approximately 4 arcsec north and south and 3 arcsec east and west of the nucleus (Figs 1 and 2). Br γ is detected at the nucleus and at 1.4 arcsec south, but the galaxy continuum is very strong and has a lot of structure, resulting in a large uncertainty for the Br γ flux.

Our nuclear emission-line spectra in the *J* and *K* bands are similar to those of Veilleux, Goodrich & Hill (1997), which were obtained with a much larger aperture (3 arcsec × 3 arcsec). The difference in aperture size may be responsible for the difference in the *K*-band continuum, which is much redder in our data. An unresolved, very red nucleus is also found in the *HST* optical continuum colour map of Mulchaey et al. (1994). Veilleux et al. (1997) report a ratio betwen the narrow Br γ and H_2 fluxes of ≈0.25, as compared with ≈0.35 in our case. They also say they may have detected broad components to Pa β and Br γ; the structure in the continuum around Br γ precludes any attempt to measure such a component in our spectra.

In Fig. 4 we show a comparison of the line profiles. The top panels show the scaled profiles from the spectra obtained with the HR grating. From the top left panel, it can be seen that the nuclear Pa β profile is very similar to that of the [Fe II]λ1.257 μm line, although the blue wing of Pa β is contaminated by [Fe II]λ1.279 μm, as described above. We do not find evidence in our data for the broad component suspected by Veilleux et al. (1997) in Pa β. As our data seems to have similar S/N to theirs, one possibility is that contamination of the blue wing of Pa β by the adjacent [Fe II] line may have been interpreted as a broad component.

Also in Fig. 4, the [Fe II] and Pa β profiles are compared with that of a He Ar (calibration lamp) line, which has FWHM = 150±5 km s^{-1}. Although the S/N is much lower for Pa β, it can be seen that both lines are much broader than the instrumental profile. The FWHMs (corrected for the instrumental FWHM above) are 520±20 km s^{-1} for [Fe II] and 430±70 km s^{-1} for Pa β. The blue and red wings of the [Fe II] line reach ≈ − 900 and 600 km s^{-1} at zero intensity, respectively. The [Fe II] profile gets narrower with increasing distance from the nucleus (top right panel of Fig. 4),

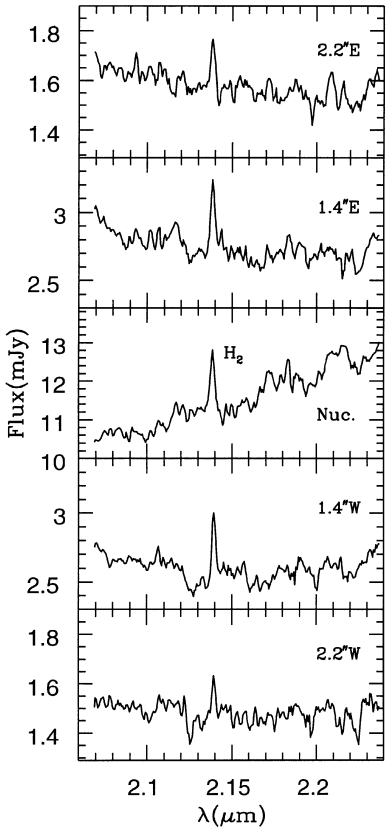

Figure 2. *K*-band spectra of NGC 2110 at $R \approx 700$ along PA = 80° (perpendicular to the radio axis), after binning two pixels (0.73 arcsec) together. The distance from the nucleus is indicated.

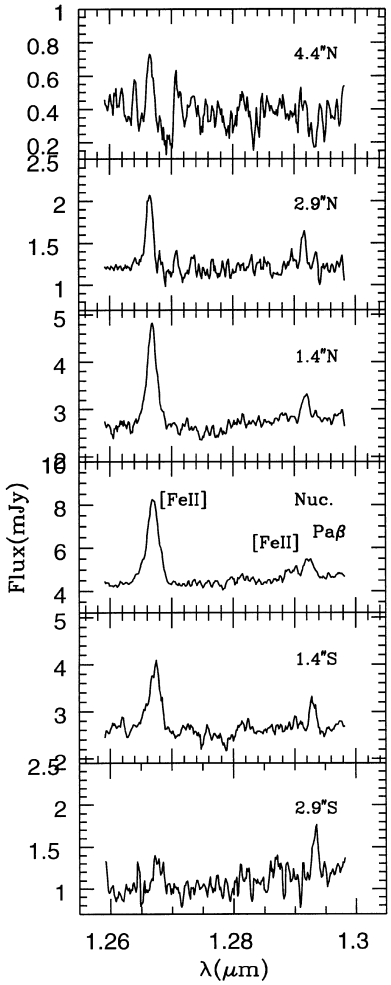

Figure 3. *J*-band spectra of NGC 2110 at $R \approx 2000$ along the radio axis at PA = 170°, after binning two pixels (0.73 arcsec) together. The distance from the nucleus is indicated.

reaching a corrected FWHM = 240±40 km s^{-1} at 2.9 arcsec north of the nucleus.

The bottom panels of Fig. 4 show the profiles from the spectra obtained with the LR grating, where it can be seen that the nuclear [Fe II] profile is still resolved. The similarity of the Paβ and [Fe II] profiles is confirmed by these data. The corrected FWHMs of [Fe II] and Paβ are, respectively, 500±40 km s^{-1} and 550±120 km s^{-1}, consistent with the values from the higher resolution spectrum. On the other hand, the nuclear H_2 profile is barely resolved, being very similar to the profiles of the Paβ and Brγ lines of the planetary nebula NGC 7009, observed as a reference, and which have observed (uncorrected) FWHM ≈ 400 km s^{-1}. Correcting the FWHM of the nuclear H_2 line for the instrumental profile (adopted as that of the Brγ line of NGC 7009), the resulting FWHM is 230±70 km s^{-1}. Finally, in the bottom right panel of Fig. 4 we present the profiles of the H_2 line as a function of distance from the nucleus, which show a marginal decrease of FWHM with increasing distance from the nucleus.

We can thus conclude that, at the nucleus of NGC 2110, the [Fe II] and H_2 lines originate in different material, the former line coming from more kinematically disturbed gas. The larger widths of the [Fe II] line could result from acceleration of interstellar gas by the radio jet, which might also be responsible for ionizing the species through the agency of shock waves (see Section 3.1.3).

3.1.2 Velocity field

Fig. 5 shows the heliocentric velocities derived from the peak wavelengths of the [Fe II]λ1.257-μm, Paβ and H_2 emission lines, from both the LR and HR data. The lower panel shows the velocities along the radio axis at PA = 170°, for all the emission lines, and the upper panel shows the velocities at PA = 80°, available only for H_2. The good agreement between the velocities derived for [Fe II] using two different gratings gives us confidence in the reliability of the data. For clarity, error bars have not been plotted in the lower panel (the sizes are similar to those in the upper panel). The adopted position of the nucleus corresponds to the peak of the continuum light in the *J* and *K* bands.

There is a small difference between the kinematics of the gas emitting [Fe II] and that emitting Paβ and H_2: the latter two emission lines show a rotation curve well represented by a circular rotation model (see below), while the [Fe II] rotation curve shows a shallower gradient near the nucleus. Although small, this difference seems to be significant (compared with the error bars in Fig. 5) and may be related to interaction of the [Fe II] emitting gas with the radio jet, already suggested by the broadening of its emission-line profile.

It is interesting to compare the near-IR and optical emission-line kinematics. Wilson & Baldwin (1985) find that the kinematic centre of NGC 2110, as derived from the optical emission-line rotation curve, is displaced 1.7 arcsec south of the optical nucleus (identified with the peak of continuum light) along PA = 161°. In order to search for any similar shifts in our data, we have fitted a model with

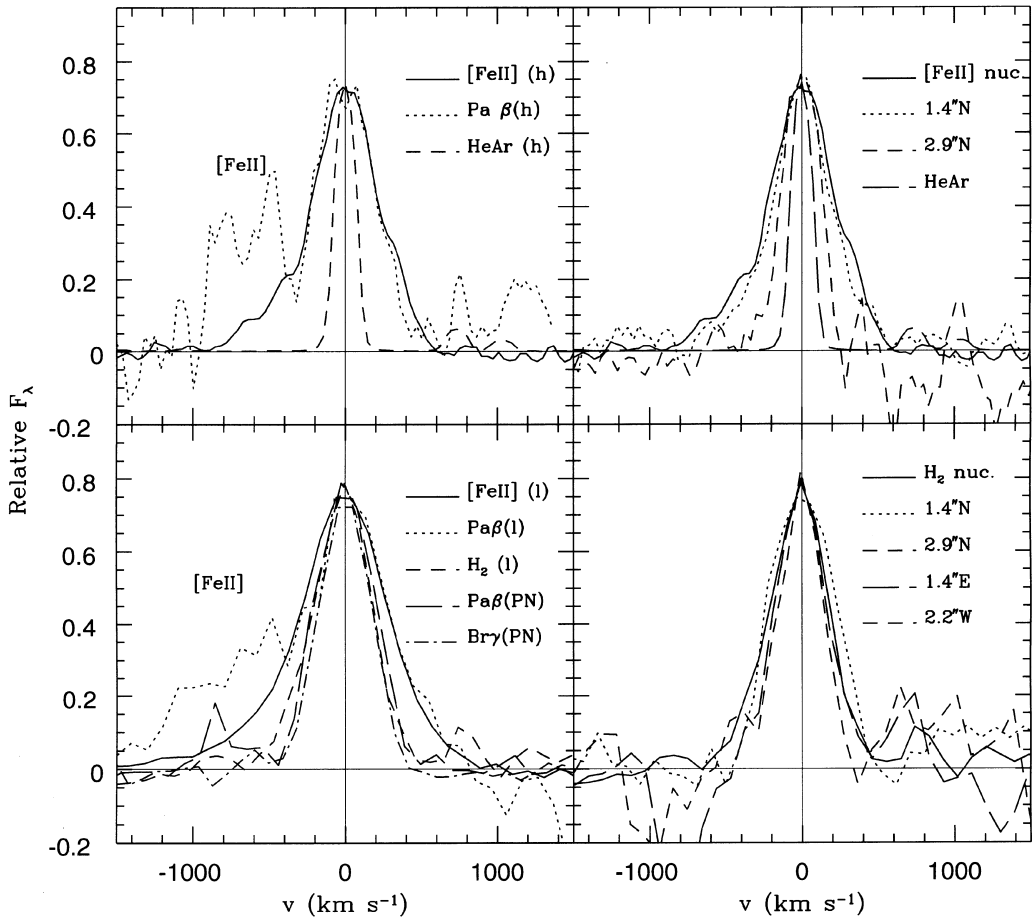

Figure 4. Comparison of the emission-line profiles of NGC 2110. The upper panels correspond to the HR grating and the lower panels to the LR grating. *Upper left:* the nuclear [Fe II]λ1.257-μm line profile (continuous line) is compared with that of Pa β (dotted line), as well as with the instrumental profile (dashed line). *Upper right:* a comparison of the [Fe II]λ1.257-μm line profiles at different distances from the nucleus along the radio axis. *Lower left:* comparison of the nuclear emission-line profiles with those of the planetary nebula NGC 7009, which are representative of the instrumental resolution. *Lower right:* comparison of the H_2 profiles as a function of distance from the nucleus.

circular rotational motions (Bertola et al. 1991) to the peak velocities of Pa β and H_2 (omitting the the [Fe II] line as its motions may be affected by interactions with the radio jet) along PA = 170°, allowing for a shift x_0 in the position of the kinematic centre with respect to the nucleus. This fit shows that the data are consistent with circular motions in the plane of the galaxy disc, with the kinematic centre shifted by $x_0 = 0.6$ arcsec south with respect to the peak of the continuum IR light. This shift is in the same direction as that from the optical observations, but is smaller. In order to investigate this diference, we have also plotted in Fig. 5 the average of the [O III] and Hβ peak velocities of Wilson & Baldwin (1985), assuming the optical and infrared nuclei coincide. The kinematic centre of this optical rotation curve is seen to be displaced $\approx$ 1.2 arcsec south relative to the kinematic centre of the IR curve.

The above results suggest that the apparent displacement between the kinematic and photometric nucleus is, at least in part, an effect of obscuration. The difference between the optical and IR rotation curves may result from either a shift between the IR and optical continuum peaks and/or the fact that the IR emission lines sample the NLR kinematics closer to the nucleus (see discussion by Wilson & Baldwin 1985 and Wilson, Baldwin & Ulvestad 1985).

3.1.3 *Emission-line fluxes and ratios*

Fig. 6 shows the line fluxes as a function of distance from the nucleus. In order to be able to compare the flux distributions along the north–south and east–west directions, we have de-projected the angular distances assuming the gas lies in the plane of the stellar disc and adopting an inclination $i = 53°$ and a major axis PA= 160° (Wilson & Baldwin 1985). The [Fe II]λ1.257-μm line fluxes obtained from the LR spectra are $\approx$ 30 per cent larger than that from the HR spectra, but when corrected for the different slit widths (1.1 arcsec for the LR and 1.7 arcsec for the HR spectra), this difference increases to a factor of 2. At least part of this difference can be attributed to a somewhat poorer seeing in the second observing run.

It can be seen in the left panels of Fig. 6 that the [Fe II] lines are more extended to the north (5 arcsec) than to the south (3 arcsec), with a small 'bump" to the north, following the radio emission. (Owing to observing constraints, it was not possbile to obtain a *J* spectrum perpendicular to the radio axis.) The Pa β flux distribution (upper right panel of Fig. 6) shows a similar extent to the north and south, being flatter to the south.

The H_2 flux distribution is presented in lower right panel of Fig. 6. After deprojection, there is no significant asymmetry in either the

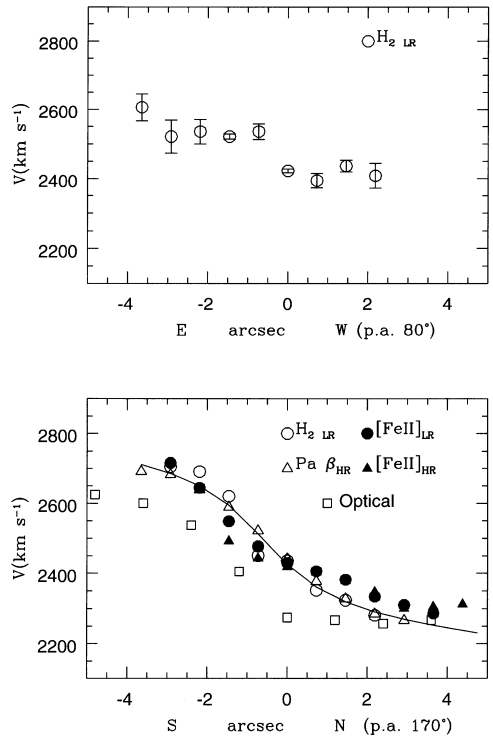

Figure 5. Heliocentric rotation curve of NGC 2110, obtained from the peak wavelengths of the emission lines. The subscripts on the labels indicate the grating used. The continuous line is the fit of a model with circular rotational motions to the Pa β and and H_2 data along PA = 170° (radio axis). For clarity, error bars have been shown only in the upper panel, but are mainly dependent on the distance to the nucleus and also apply approximately to the lower panel. The average peak velocities from [O III]λ5007 and Hβ (Wilson & Baldwin 1985) are represented by open squares.

north–south or east–west H_2 flux distributions within 3 arcsec of the nucleus. The H_2 line is detected further from the nucleus along the east–west direction than along the north–south direction. Although a compact molecular torus may contribute to the H_2 emission, the line extends to $\approx$1 kpc from the nucleus. Moreover, the H_2 kinematics are consistent with circular motion in the disc of the galaxy (Section 3.1.2).

The luminosity in the H_2 line can be used to estimate the mass of hot molecular hydrogen in NGC 2110. We have used the method described by Veilleux et al. (1997), which is based on the calculations of Scoville et al. (1982). Adopting cylindrical symmetry for the H_2 flux distribution, we obtain an integrated H_2 $v = 1$–0 S(1) luminosity in the inner 10 arcsec (Fig. 6) of $L_{H_2} = 6.7 \times 10^{39}$ erg s^{-1}. If the hot H_2 molecules are thermalized at $T = 2000$ K, and assuming that the power in all H_2 lines is 10 times that in the S(1) line, this luminosity translates into a hot H_2 mass of 2 300 $M_\odot$. If we correct the H_2 luminosity for extinction [adopting $E(B-V) = 1.5$ – see below] the luminosity and resulting mass would be $\approx$ 60 per cent larger.

The emission-line ratio [Fe II]λ1.257/Pa β as a function of distance from the nucleus along the radio axis is presented in Fig. 7. It reaches very high values at the nucleus: $\approx$7, much higher than the value of $\approx$1 found in NGC 1068, for example (Ward et al. 1987). It decreases more slowly to the north (along the radio emission) than to the south, and only in the outermost regions of NGC 2110 does this ratio approach unity.

The origin of the [Fe II] emission in Seyfert galaxies has been extensively discussed in previous works (e.g. Forbes & Ward 1993; Simpson et al. 1996a; Veilleux et al. 1997). Possibilities include ionization by X-rays from the central source, ionization by shocks produced by interaction of a radio jet with the surrounding medium, and contributions from starbursts. However, detailed calculations by Colina (1993) show that, for starbursts, [Fe II]/Pa β $\leq$0.4, suggesting a starburst contribution is not important for the nuclear region of NGC 2110. Forbes & Ward (1993) favour ionization by shocks in both starbursts and Seyferts because of the correlation between [Fe II] and radio fluxes, which was confirmed by the additional data of Veilleux et al. (1997). For NGC 2110 the broadening of the [Fe II] profile (discussed above) at the locations where the [Fe II]λ1.257/Pa β ratio is higher, the presence of a linear radio source and the fact that the [Fe II] emission is more extended along the radio axis give further support to this scenario. The very high nuclear [Fe II]λ1.257/Pa β ratio can thus be understood as resulting from the fact that while both Pa β and [Fe II] likely contain contributions from photoionization by the central source, the [Fe II] emission is further enhanced by the shock ionization of Fe by the radio jet.

For the nucleus, we obtain the ratio H_2 $v = 1$–0 S(1)/Br $\gamma \approx 3.0 \pm 2.0$; it was not possible to measure Br γ outside the nucleus. The ratio H_2 $v = 1$–0 S(1)/Br γ allows us to discriminate between various excitation mechanisms for the H_2 emission. In star-forming regions, where the main heating agent is UV radiation, H_2/Brγ < 1.0, while for Seyferts this ratio is larger because of additional H_2 emission excited by shocks or by X-rays from the active nucleus (Moorwood & Oliva 1994). For NGC 2110, although some contribution from shocks cannot be discarded, the smaller width of the H_2 emission line when compared with that of the [Fe II]λ1.257 suggests that the excitation of H_2 is dominated by X-rays from the active nucleus. Veilleux et al. (1997) have shown that NGC 2110 has enough X-ray emission to produce the necessary excitation.

3.1.4 *Reddening and dust emission*

The ratio between the Br γ and Pa β nuclear fluxes can be used to estimate the gaseous reddening at the nucleus under the assumption of Case B recombination (for $T = 10^4$ K, Br γ/Pa β= 0.170; Osterbrock 1989) and the reddening law from Whitford (1958) and Rieke & Lebofsky (1985), through the expression

$$E(B-V) = 5.21 \times \log\left(\frac{(F_{\mathrm{Br}\gamma}/F_{\mathrm{Pa}\beta})}{0.170}\right) \mathrm{mag}.$$

The resulting nuclear reddening, after subtraction of the foreground Milky Way reddening $E(B-V)_G \approx$ 0.36 mag (Burstein & Heiles 1982), is $E(B-V) = 1.1 \pm 0.7$ mag. This reddening is comparable with a previous optical determination [$E(B-V) = 0.73$ mag – Shuder 1980]. The error is large because of the uncertainties in the fluxes of Br γ and Pa β [$F_{\mathrm{Br}\gamma} = 1.0(\pm0.4) \times 10^{-15}$ erg cm^{-2} s^{-1}; $F_{\mathrm{Pa}\beta} = 3.0(\pm0.4) \times 10^{-15}$ erg cm^{-2} s^{-1}; both integrated over an area of 1.1 arcsec $\times$ 0.73 arcsec].

The nuclear reddening can also be estimated from the slope of the continuum. We have used the spectra of Fig. 1 to obtain the $J-K$ colours: after correcting for $E(B-V)_G$, we obtain $J-K \approx 1.9$ mag for the nucleus and $\approx$0.9 mag for the extranuclear spectra. The nuclear value is in good agreement with the colours $J-H = 0.93$ and $H-K = 1.0$ obtained by Alonso-Herrero et al. (1998) within an aperture of 1.5 arcsec diameter. If the intrinsic nuclear colour were the same as that of the extranuclear regions and the observed colour were a result of reddening of the starlight by dust, the nuclear obscuration would be $A_V \approx$ 6 mag, larger than the value obtained from the emission lines.

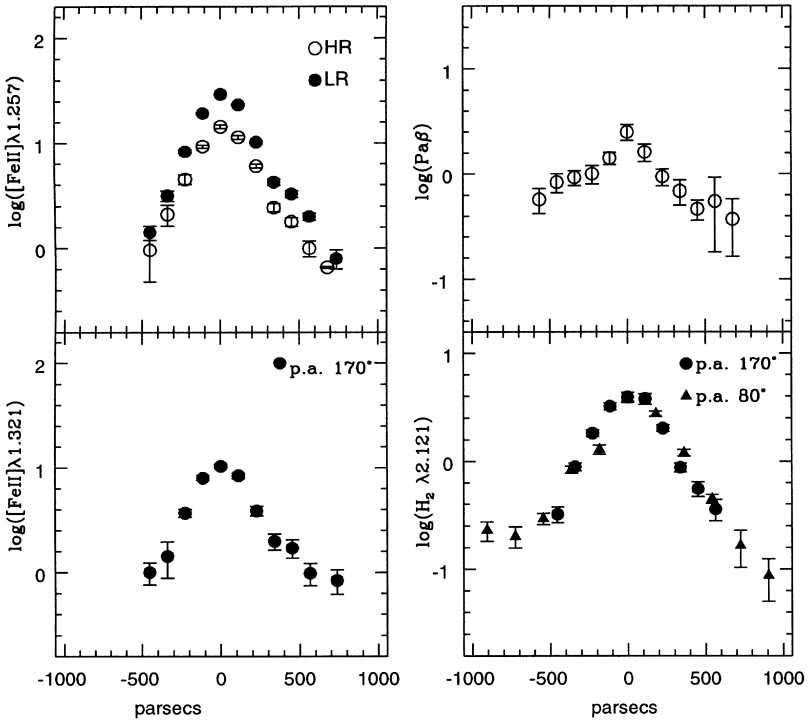

Figure 6. Logarithm of the emission-line fluxes (in units of 10^{-15} erg cm^{-2} s^{-1} arcsec^{-2}) as a function of distance from the nucleus of NGC 2110. Circles correspond to the direction south–north (radio axis), with south negative and north positive. Triangles correspond to the direction east–west, with E negative and W positive. The x-axes refer to distances in the plane of the galaxy disc (scale: 151 pc arcsec^{-1}), assuming $i = 53°$ and major axis PA=160°. Open symbols correspond to the HR grating, and filled symbols to the LR grating.

On the other hand, $J - K \approx 2$ is also consistent with a mixture of a late-type stellar population and emission by hot dust (Simpson et al. 1996b). In order to investigate whether obscuration or dust emission is responsible for the red nuclear colour of NGC 2110, we have compared the slopes of the nuclear continuum in our J- and K-band spectra with those of the extranuclear continua reddened by various values. In the J band the slope of the nuclear continuum is very similar to that of the extranuclear continua, and is consistent with a nuclear $E(B-V) < 1.1$. In the K band, however, the continuum at the nucleus is much steeper (redder) than in the extranuclear spectra, implying $E(B-V) \geq 3$, in disagreement with the low reddening of the J band.

We also find that extrapolation of the J-band spectrum to the K band gives a continuum flux at $\lambda \approx 2.07$ μm in agreement with that observed. At longer wavelengths, the spectrum is much redder, suggesting we are seeing another component. According to models (e.g. Pier & Krolik 1993), this spectral region corresponds to the onset of the emission from a dusty torus heated by the active galactic nucleus (AGN). In fact, we have successfully fitted a simple blackbody curve to the nuclear K-band spectrum, but the temperature depends on the contribution of other components, such as the underlying galaxy spectrum. For example, subtracting a constant contribution at the K-band of 85 per cent at λ2.15 μm, for these components, we obtain a blackbody temperature of $T = 730$ K. We thus conclude that the red nuclear continuum is most probably a result of hot dust emission. This red continuum is only present in the nuclear spectrum, and is not resolved (size < 150 pc), consistent with the torus hypothesis.

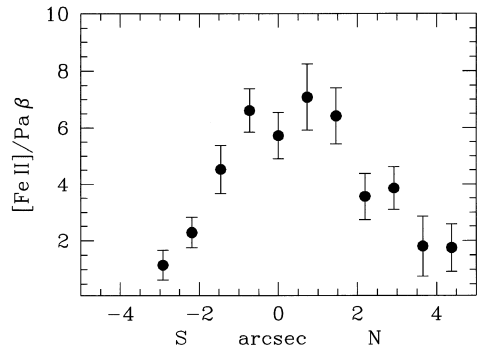

Figure 7. Emission-line ratio [Fe II]λ1.257/Pa β as a function of distance from the nucleus of NGC 2110 along the radio axis at PA = 170°. Negative positions are to the south and positive to the north.

3.2 Circinus

3.2.1 Emission-line profiles

Fig. 8 shows the J and K spectra of the Circinus galaxy obtained with the HR grating along PA = 24° (close to the galaxy major axis), while Fig. 9 shows the spectra along PA = −66° (close to the radio axis). Emission in the lines [Fe II]λ1.257 μm, Pa β, H_2 $v = 1$–0 S(1) and Br γ extends beyond the central 15 arcsec covered by the slit, while the coronal line of [S IX] at λ1.252 μm is spatially unresolved (≤ 1 arcsec; 19 pc), as previously found by Oliva et al. (1994), and consistent with modelling by Binette et al. (1997).

The emission lines are barely resolved spectrally, as illustrated in Fig. 10, where the profiles of [S IX], [Fe II]λ1.257 μm and Pa β in the nuclear J spectrum are shown together with the profile of a comparison lamp emission line. When corrected by the instrumental profile, the FWHMs of these emission lines are 97, 143 and 133 km s^{-1}, respectively. The uncertainties are large (30–50 km s^{-1}) because the uncorrected FWHM values are close to the instrumental value (150 km s^{-1}). A common characteristic of all

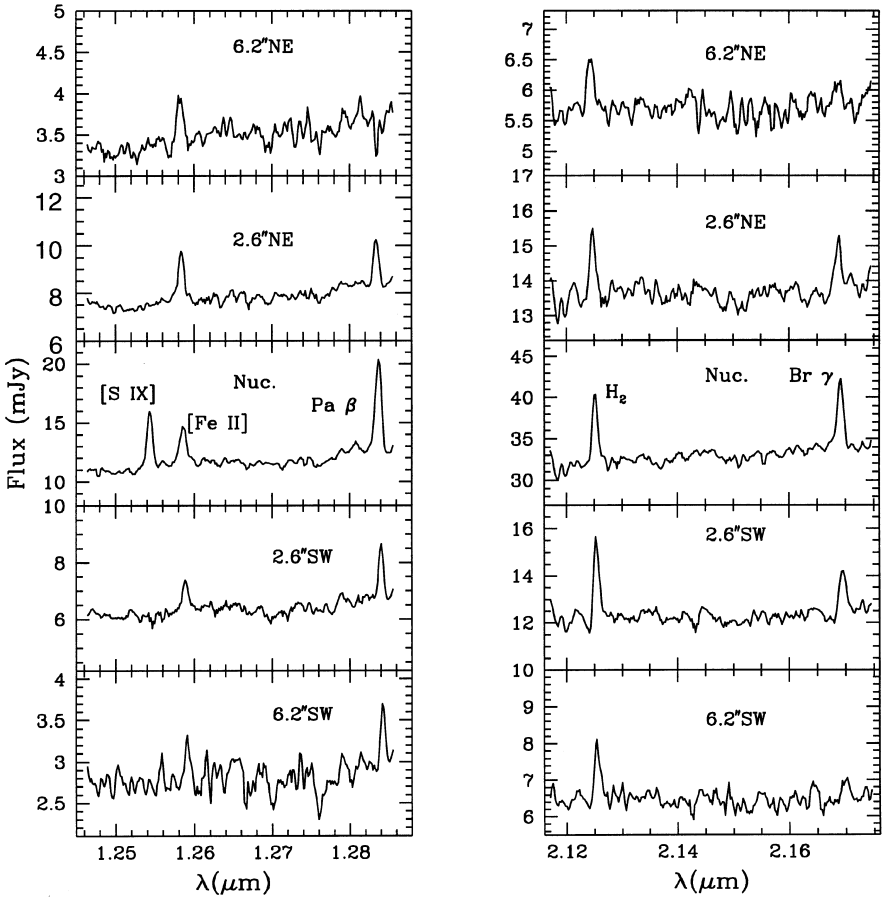

Figure 8. *J*- and *K*-band spectra of Circinus at $R \approx 2000$ along the galaxy plane at PA = 24° after binning two pixels (0.73 arcsec) together. The distance from the nucleus is indicated.

the nuclear emission-line profiles is a slight blueward-slanting asymmetry.

3.2.2 *Velocity field*

Fig. 11 shows the heliocentric gas velocities of Circinus, obtained from the peak wavelengths of [Fe II]λ1.257 μm and Pa β along PA = 24° and PA = −66° . Also shown is the fit of a model with circular rotational motions (Bertola et al. 1991) to the data along PA = 24°. As in the case of NGC 2110, the velocity field is dominated by circular rotation in the plane of the galaxy, and the kinematic centre is displaced 1.0 arcsec south-west of the peak of the IR continuum. Our data can be compared with IR and optical data from Maiolino et al. (1998), also shown in Fig. 11 as open squares: the inner five points correspond to stellar features in the *K* band, and the outermost points to optical emission in [N II]λ6584. Our results agree with those of Maiolino et al., filling nicely the gaps in their data.

3.2.3 *Emission-line fluxes and ratios*

Fig. 12 shows the line fluxes as a function of distance from the nucleus, along PA = 24° (major axis) and PA = −66° (radio axis). The [Fe II]λ1.257-μm emission is, on average, stronger along the radio axis than along the galaxy axis. The H_2 and Br γ fluxes at the nucleus in the spectrum obtained along the radio axis are about 50 per cent of the corresponding values in the spectrum obtained along the galaxy major axis, which suggests that the slit was not well centred in the *K* spectrum along PA = −66°.

We have compared our flux distributions with the emission-line images of Davies et al. (1998, hereafter D98) in H_2 and [Fe II]λ1.64 μm. The latter line comes from the same upper level as [Fe II]λ1.257 μm (having intrinsically 75 per cent of its flux), and we can thus compare the two brightness distributions.

The H_2 brightness distribution of D98 shows a central peak, corresponding to a marginally resolved central source, with a steep radial profile, superimposed on extended emission with a shallower radial profile. From the lower left panel of Fig. 12, it can be seen that our H_2 fluxes present a similar behaviour, showing a steeper flux distribution within 2 arcsec from the peak (which seems to be located ≈ 1 arcsec to the southwest and southeast of the peak in the continuum) than in the outer parts.

The [Fe II] flux distribution of D98 is less centrally peaked, showing an extension between north and north-east. Our [Fe II]λ1.257-μm flux distribution consistently shows a 'flat top' along PA 24°. However, along the radio axis, our data are as extended as along PA 24°, while D98 conclude that the [Fe II] emission is less extended towards the cone.

The integrated $H_2\, v = 1\text{–}0, S(1)$ luminosity in the inner ≈13 arcsec (Fig. 12) is 4.3×10^{38} erg s^{-1}, which translates into a hot H_2 mass of 140 $M_\odot$, using the same assumptions as for NGC 2110. Allowing for an average reddening of $E(B-V) \approx 2.5$ (see below), the above luminosity and mass increase by a factor of ≈2.2.

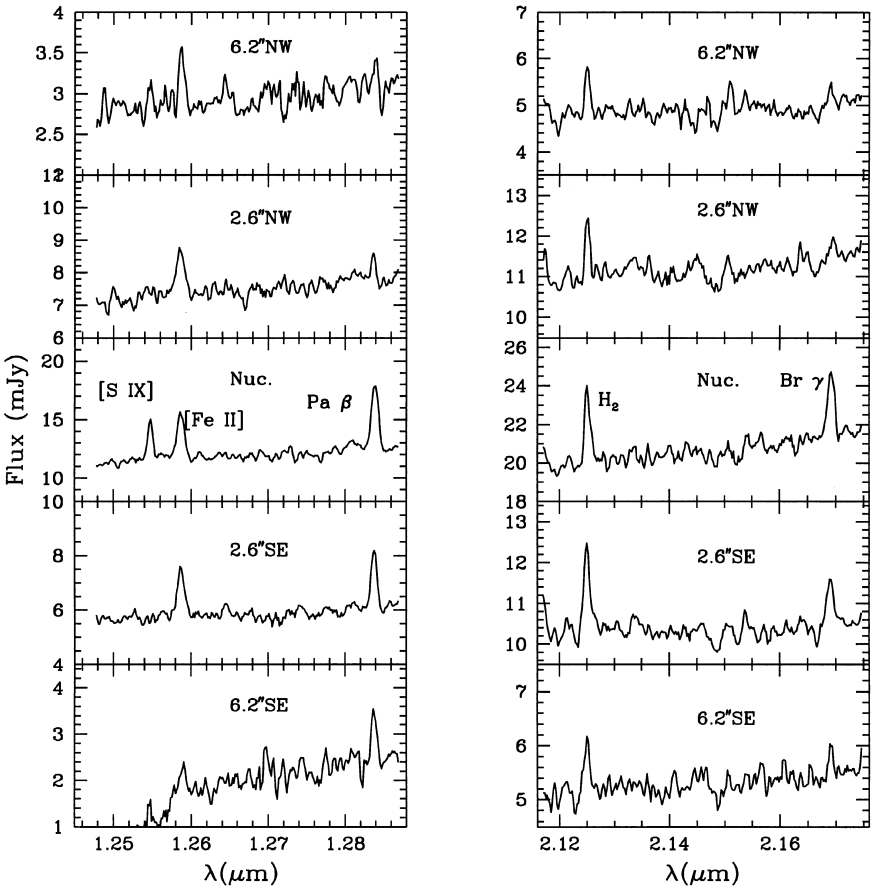

Figure 9. *J*- and *K*-band spectra of Circinus at $R \approx 2000$ along the radio axis at PA = −66° after binning two pixels (0.73 arcsec) together. The distance from the nucleus is indicated.

Fig. 13 shows the line ratios [Fe II]λ1.257/Pa β and H_2/Br γ along PA = 24° and −66°. [Fe II]/Pa β has the value of 0.4 at the nucleus and increases outwards, most notably along the radio axis, reaching values larger than 2. H_2/Br γ presents a similar behaviour: it is ≈1 at the nucleus and increases outwards to values larger than 2. Both ratios at the nucleus have values typical of starbursts (see discussion above for NGC 2110), suggesting that the starburst dominates the gaseous excitation there. The larger ratios away from the nucleus suggest that X-ray radiation from the active nucleus and/or shocks dominate the excitation. In particular, the high [Fe II]λ1.257/Pa β ratios may trace the high-excitation gas, which extends along the galaxy minor axis as shown by the 'ionization map' (optical line ratio map [O III]/(Hα+[N II]) of Marconi et al. (1994).

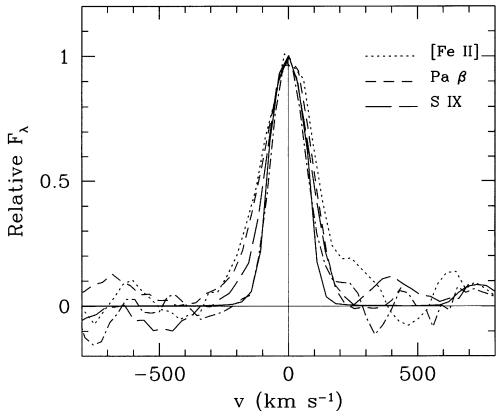

Figure 10. Comparison of the nuclear emission-line profiles of Circinus with the instrumental profile (continuous line).

Our results regarding the nature of the H_2 emission seem to contradict the interpretation put forward by D98. They argue that the nuclear H_2 component has the flux expected from excitation produced by the observed nuclear X-ray flux, and thus may originate from gas in the molecular torus excited by the nuclear AGN, while the more extended emission could be caused by ongoing star formation. Our results suggest that the opposite is true (see Fig. 13, right panel).

3.2.4 *Reddening and dust emission*

We have used the line fluxes in Pa β and Br γ to obtain the gaseous reddening along PA = 24° (we did not calculate the reddening along PA = −66° because of the apparent misplacement of the slit in the *K*-band spectrum at this PA). After correction for the foreground Milky Way reddening $E(B-V)_G = 0.5$ mag (Freeman et al. 1977), the internal reddening lies in the range $1 \leq E(B-V) \leq 3.5$ mag, and increases from northeast to southwest, as shown in Fig. 14.

The continuum colour [corrected for $E(B-V)_G$] is reddest at the nucleus, where $J-K = 1.9$, decreasing to $J-K \approx 1.3$ to the northeast, and to $J-K \approx 1.5$–1.6 to the southwest.

On the assumption that the reddening derived from the emission lines can be applied to the continuum, we obtain intrinsic colours

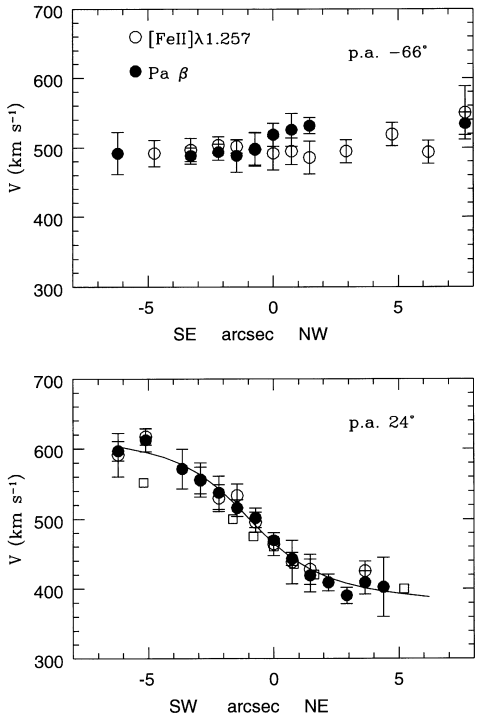

Figure 11. Rotation curve of Circinus, obtained from the peak wavelength of the emission lines. The continuous line represents the fit of a model with circular rotational motions to the data along the galaxy plane at PA = 24°. Squares represent data from Maiolino et al. (five inner points from *K*-band stellar absorption features and the two outermost points from the optical [N II]λ6584 emission line).

$J-K$ in the range 0.4–0.8 for the extranuclear spectra and $J-K \approx 1$ for the nuclear spectrum. The former $J-K$ colours are typical of starbursts of ages 10^6–10^8 yr (Leitherer & Heckman 1995). This result is in agreement with the modelling of Maiolino et al. (1998), who concluded that, on the basis of a Br γ emission map, within 100 pc from the nucleus the stellar population has an age ranging between 4×10^7 and 1.5×10^8 yr.

4 SUMMARY AND CONCLUDING REMARKS

Long-slit spectra in the near-IR *J* and *K* bands of the Seyfert 2 galaxies NGC 2110 and Circinus have revealed extended emission in [Fe II]λ1.257 μm, Pa β and H_2 $v = 1$–0 S(1) up to at least ≈ 900 pc (6 arcsec) from the nucleus in NGC 2110 and beyond the end of the slit – 130 pc (7 arcsec) from the nucleus – in the case of Circinus.

The profiles of the emission lines [Fe II]λ1.257 μm and Pa β from the nucleus of NGC 2110 are broad (FWHM ≈ 500 km s^{-1}) and quite similar, while the profile of H_2 $v = 1$–0 S(1) is narrower, with FWHM ≤ 300 km s^{-1}, and thus originates in a kinematically less disturbed gas. We do not confirm previous reports of a very broad Pa β component. In Circinus, the profiles are barely resolved spectrally, with FWHM ≤ 150 km s^{-1}.

The H_2 line luminosities and masses of hot molecular gas are similar to those of other Seyfert galaxies (e.g. Veilleux et al. 1997). The [Fe II]λ1.257-μm emission may trace the high-excitation gas. In the case of NGC 2110, the high [Fe II]λ1.257-μm/Pa β flux ratio combined with the broadening of the nuclear profiles suggests that shocks (perhaps driven by the radio jet) are an important source of excitation of the [Fe II] emission. The high H_2 $v = 1$–0 S(1)/Br γ nuclear ratio, combined with the smaller width of the H_2 emission line, suggests that the excitation of the H_2 line is dominated by

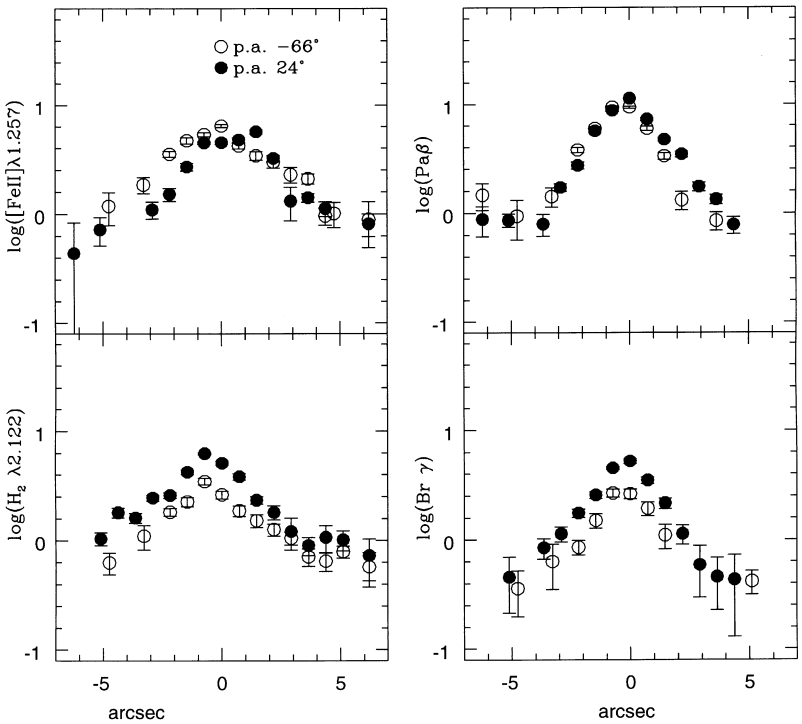

Figure 12. Logarithm of the emission-line fluxes of Circinus (in units of 10^{-15} erg cm^{-2} s^{-1} arcsec^{-2}] as a function of distance from the nucleus, along the galaxy plane at PA = 24° (filled circles) and along the radio axis at PA = −66° (open circles). For p.a = 24°, south-west is negative and north-east positive. For PA = −66°, south-east is negative and north-west positive.

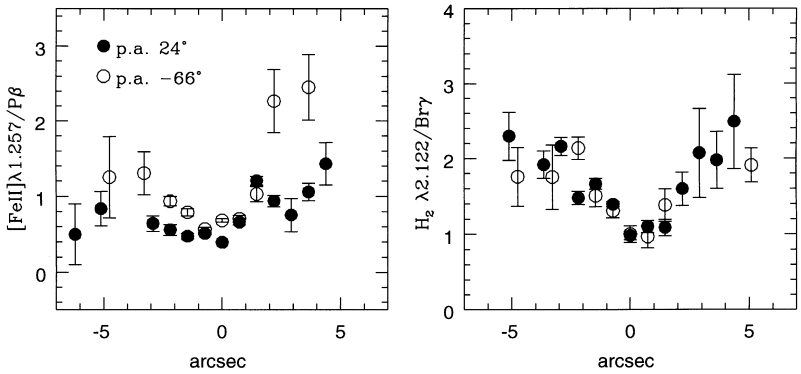

Figure 13. Emission-line ratios of Circinus as a function of distance to the nucleus along the galaxy plane at PA = 24° (filled circles) and along the radio axis at PA = −66° (open circles). Along PA = 24°, south-west is negative and north-east positive. Along PA = −66°, south-east is negative and north-west positive.

X-ray emission from the active nucleus. In the case of Circinus, the much lower ratios at the nucleus are similar to those observed for starbursts, suggesting that the nuclear starburst is the main source of excitation there. However, a few arcsec away from the nucleus these ratios increase to values similar to those found in Seyfert nuclei, showing that the radiation of the active nucleus may be the main source of excitation outside the nucleus.

We were able to obtain rotation curves in the IR lines for both galaxies, which indicate that the gaseous kinematics is dominated by circular motions in the discs of the galaxies. In both cases we found a displacement between the peak of the IR continuum and the kinematic center of the galaxy along the PA closest to the major axis. In the case of NGC 2110, this effect had been previously found using optical observations, but the IR rotation curve is more symmetric relative to the nucleus than the rotation curve obtained from optical lines. This result suggests that the offset of the continuum nucleus with respect to the kinematic centre is, at least in part, an effect of obscuration.

For NGC 2110, $J-K \approx 0.9$ everywhere, except right at the nucleus, where $J-K \approx 1.9$. The continuum spectrum within the K band is very steep and cannot be explained by reddening alone. The observations clearly show that we are seeing another component in emission in the K band, which is consistent with the expected emission of dust heated by an AGN. This emission is unresolved in our data (0.73 arcsec × 1.1 arcsec), and may originate in the walls of a circumnuclear dusty torus.

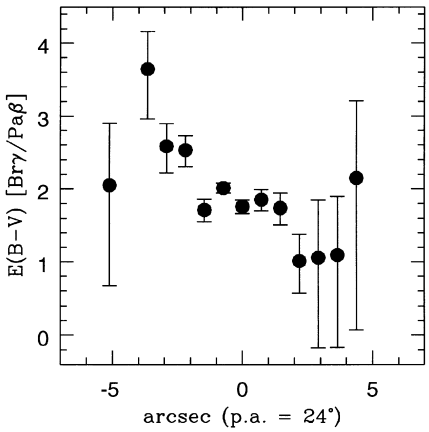

Figure 14. Reddening $E(B-V)$ (in mag) as a function of distance from the nucleus of Circinus along the galaxy plane at PA = 24°. South-west is negative and north-east positive.

For Circinus, the Br γ/Pa β ratios indicate gaseous reddening in the range $1 \leq E(B-V) \leq 3$. The $J-K$ values are consistent with those of an ageing starburst with the same reddening as the emitting gas, except at the unresolved nucleus, which has a redder colour.

ACKNOWLEDGMENTS

We thank the staff of CTIO for their support and assistance with the near-IR observations and reductions, in particular Richard Elston. We also thank the referee, Chris Done, for several suggestions which helped to improve the paper. This work was partially supported by the Brazilian institutions CNPq, FAPERGS and FINEP. This research has made use of the NASA/IPAC Extragalactic Database (NED), which is operated by the Jet Propulsion Laboratory, under contract with NASA.

REFERENCES

Alonso-Herrero A., Ward, M. J., Kotilainen J. K., 1996, MNRAS, 278, 902
Alonso-Herrero A., Simpson C., Ward M. J., Wilson A. S., 1998, ApJ, 495, 196
Antonucci R. R. J., 1993, ARA&A, 31, 473
Antonucci R. R. J., Miller J. S., 1995, ApJ, 297, 621
Bertola F., Bettoni D., Danziger J., Sadler E., Sparke L., de Zeeuw T., 1991, ApJ, 373, 369
Binette L., Wilson A. S., Raga A., Storchi-Bergmann T., 1997, A&A, 327, 909
Blietz M., Cameron M., Drapatz S., Genzel R., Krabbe A., van der Werf P., Sternberg A., Ward M., 1994, ApJ, 421, 92
Bradt H. V., Burke B. F., Canizares C. R., Greenfield P. S., Kelly R. L., McClintock J. E., Van Paradijs J., Koski A. T., 1978, ApJ, 226, L111
Burstein D., Heiles C., 1982, AJ, 87, 1165
Cid Fernandes R., Storchi-Bergmann T., Schmitt H., R. 1998, MNRAS, 297, 259
Colina L., 1993, ApJ, 411, 565
Davies R. I. et al., 1998, MNRAS, 293, 189 (D98)
Elias J. H., Frogel J. A., Matthews K., Neugebauer G., 1982, AJ, 87, 1029
Elmoutie M., Haynes R. F., Jones K. L., Ehle M., Beck R., Wielebinski R., 1995, MNRAS, 275, L53
Forbes D. A., Ward M. J., 1993, ApJ, 416, 150
Freeman K. C., Karlsson B., Lynga G., Burrell J. F., van Woerden H., Goss W. M., Mebold U., 1977, A&A, 55, 445
Leitherer C., Heckman T. M., 1995, ApJS, 96, 9
McAlary C. W., Rieke G. H., 1988, ApJ, 333, 1
Maiolino R., Krabbe A., Thatte N., Genzel R., 1998, ApJ, 493, 650
Marconi A., Moorwood A. F., Origlia L., Oliva E., 1994, ESO Messenger, 78, 20

Moorwood A. F. M., Oliva E., 1988, A&A, 203, 278
Moorwood A. F. M., Oliva E., 1990, A&A, 239, 78
Moorwood A. F. M., Oliva E., 1994, ApJ, 429, 602
Moorwood A. F. M., van der Werf P. P., Kotilainen J. K., Marconi A., Oliva E., 1996, A&A, 308, 1
Mulchaey J. S., Wilson A. S., Bower G. A., Heckman T. M., Krolik J. H., Miley G. K., 1994, ApJ, 433, 625
Mulchaey J. S., Wilson A. S., Tsvetanov Z. I., 1996, ApJS, 102, 309
Oliva E., Salvati M., Moorwood A. F. M., Marconi A., 1994, A&A, 288, 457
Osterbrock D. E., 1989, Astrophysics of Gaseous Nebula and Active Galactic Nuclei. University Science Books, Mill Valley, CA
Pier E. A., Krolik J. H., 1993, ApJ, 418, 673
Rieke G. H., Lebofsky M. J., 1985, ApJ, 288, 618
Sanders D. B., Phinney E. S., Neugebauer G., Soifer B. T., Matthews K., 1989, ApJ, 347, 29
Scoville N. Z., Hall D. N. B., Kleinmann S. G., Ridgway S. T., 1982, ApJ, 253, 136
Shuder J. M., 1980, ApJ, 240, 32
Simpson C., Forbes D. A., Baker A. C., Ward M. J., 1996a, MNRAS, 283, 777
Simpson C., Mulchaey J. S., Wilson A. S., Ward M. J., Alonso-Herrero A., 1996b, ApJ, 457, L19
Storchi-Bergmann T., Wilson A. S., Baldwin J. A., 1992, ApJ, 396, 45
Storchi-Bergmann T., Kinney A. L., Challis P., 1995, ApJS, 98, 103
Storchi-Bergmann T., Wilson A. S., Baldwin J. A., 1996, ApJ, 460, 252
Ulvestad J. S., Wilson A. S., 1983, ApJ, 264, L7
Veilleux S., Goodrich R. W., Hill G. J., 1997, ApJ, 477, 631
Ward M. J., Geballe T., Smith M., Wade R., Williams P., 1987, ApJ, 316, 138
Whitford A. E., 1958, AJ, 63, 201
Wilson A. S., Baldwin J. A., 1985, ApJ, 289, 124
Wilson A. S., Baldwin J. A., Ulvestad J. S., 1985, ApJ, 291, 627

This paper has been typeset from a TEX/LATEX file prepared by the author.